We are IntechOpen, the world's leading publisher of Open Access books
Built by scientists, for scientists

6,900
Open access books available

185,000
International authors and editors

200M
Downloads

154
Countries delivered to

Our authors are among the

TOP 1%
most cited scientists

12.2%
Contributors from top 500 universities

CLARIVATE ANALYTICS
BOOK CITATION INDEX
INDEXED

WEB OF SCIENCE™

Selection of our books indexed in the Book Citation Index
in Web of Science™ Core Collection (BKCI)

Interested in publishing with us?
Contact book.department@intechopen.com

Numbers displayed above are based on latest data collected.
For more information visit www.intechopen.com

Fabrication of 3-D Structures Utilizing Synchrotron Radiation Lithography

Mitsuhiro Horade and Susumu Sugiyama
Ritsumeikan University
Japan

1. Introduction

Microfabrication of high-aspect-ratio or three-dimensional (3-D) structures is critical for the production of various components for micro electro mechanical systems (MEMS). The term "three-dimensional structure" refers to a structure with a free-form surface or sloped sidewall. This article describes the fabrication of 3-D microstructures using synchrotron radiation (SR) lithography. SR lithography technology is one component of the LIGA process, and it is also called X-ray lithography.

MEMS devices have attracted a great deal of attention, and further studies are needed to realize their full potential. Among fabrication technologies, microfabrication, developed using a semiconductor process, is in high demand. Recently, the demand for MEMS devices has diversified, and microfabrication technologies for the production of high-aspect-ratio and 3-D structures are required to meet this demand.

Microfabrication technologies for the production of high-aspect-ratio structures include deep reactive-ion etching (D-RIE) and deep X-ray lithography in the LIGA process utilizing SR light. In the former, because SR light is highly directional, it is possible to fabricate a structure with a thickness of several hundred to one thousand micrometers. Moreover, because SR light contains X-ray (short wavelength) regions, it is possible to transfer patterns that are ≤ 1 μm (diffraction during exposure does not occur readily). Therefore, SR lithography has been used as a fabrication technology for high-aspect-ratio structures. It is possible to fabricate high-aspect-ratio structures using D-RIE. However, because a patterned, indented sidewall called a scallop is formed due to the nature of the process mechanism, it is difficult to fabricate structures with smooth sidewall surfaces. On the other hand, it is possible to fabricate structures with smooth sidewall surfaces using SR lithography, which is discussed in more detail in Chapter 2.

In the field of 3-D microfabrication, techniques such as KOH anisotropic etching of silicon and laser machining have been employed (Tsukada et al., 2005). However, 3-D fabrication using SR lithography was recently achieved, and results have already been reported (Horade & Sugiyama, 2009; Lee & Lee, 2003; Matsuzuka et al., 2005; Mekaru et al., 2007; Sugiyama et al., 2004; Tabata et al., 2000). Nanoscale 3-D microfabrication technology using SR lithography can be used to fabricate high-aspect-ratio structures by exploiting the properties of SR, and free-form structures with inclined sidewall surfaces can be fabricated. Additionally, this article describes 3-D polytetrafluoroethylene (PTFE) microstructures fabricated by SR ablation. Because PTFE is a remarkable material, there are high

expectations regarding its application in various devices. PTFE fabrication by SR ablation is discussed in detail in Chapter 4.

2. SR lithography

This section outlines the LIGA process, the fabrication mechanism of SR lithography, and optimum experimental conditions. To achieve high-accuracy microfabrication, optimum exposure and development conditions were determined using both experimental and theoretical values. Energy distribution, etching rate, control of processing depth, and micro-loading effects are described.

2.1 LIGA process

The LIGA process fabricates microstructures as components of MEMS (Figure 1). As shown in Figure 1, resist materials are first exposed using a soft X-ray source from an SR light through the mask, and the exposed resists are then developed. The exposure and development processes are discussed in more detail in Sections 2.2 and 2.3. Next, metallic moulds, such as Ni, are fabricated using an electroforming technique. Resist is then removed from the metallic moulds. In this process, it is possible to remove the resist under pressure as well as dissolve the resist using wet etching. Finally, microstructures of various materials are fabricated by moulding. The LIGA process can be applied to a wide range of materials, including plastics, metal, and ceramics, when the electroforming technique and moulding process are utilized.

This technology was developed in the 1980s by a group of researchers led by Becker and Ehrfeld of the Kernforschungszentrum Karlsruhe (KfK). LIGA is a German acronym consisting of the initial letters of three processes: lithographie (lithography), galvanoformung (electroforming), and abformung (moulding).
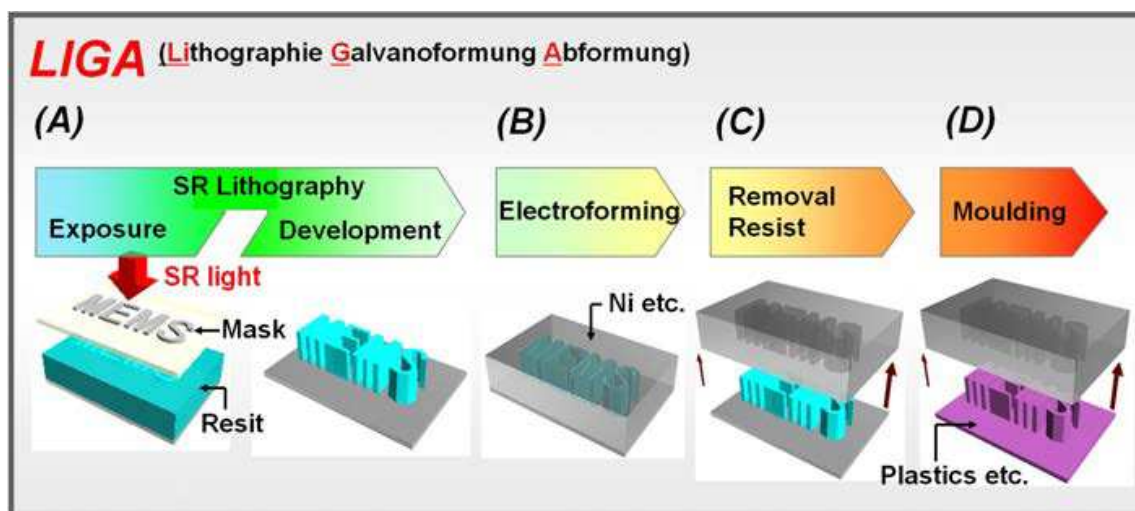

Fig. 1. Process flow of the LIGA process; (A) SR lithography; (B) electroforming; (C) removal resist; and (D) moulding

Next, we describe the characteristics of the LIGA process. Because SR light is highly directional, it is possible to fabricate a structure with a thickness of several hundred to one thousand micrometers. Moreover, because SR light contains X-ray (short wavelength)

regions, it is possible to transfer patterns that are ≤ 1 μm (diffraction during exposure does not occur readily). Therefore, SR lithography has been used as a fabrication technology for high-aspect-ratio microstructures. Fabrication of Ni structures with a line width of 2 μm and an aspect ratio of 100 or a line width of 0.2 μm and an aspect ratio of 75 have been reported (Kato et al., 2007; Kondo et al., 2000; Ueno et al., 2000). Although it is also possible to transfer patterns that are ≤ 1 μm using electron beam lithography, it has the disadvantage of a long exposure time. On the other hand, because the production of large volumes is possible using electroforming and moulding in the LIGA process, it is a superior technology in terms of time and cost.

2.2 Exposure
2.2.1 Light source

In SR lithography, the use of ultra-bright and highly directional SR light sources provides perfect conditions for fabricating structures with the required thickness. Although SR light is spectrally continuous and includes a wide wavelength range, wavelengths of 0.2 to 0.5 nm are most suitable for SR lithography because they reduce the spread of light by Fresnel diffraction in the long-wavelength domain and the generation of secondary electrons inside resists in the short-wavelength domain, enhancing resolution.

Experiments described in this article utilized the superconductivity compact SR source "AURORA" at the SR Centre of Ritsumeikan University in Japan (Figure 2). The properties of SR at AURORA include a wavelength range from 0.15 nm to visible light and an applied electron energy and maximum storage current of 575 MeV and 300 mA, respectively. This light source was adapted for our studies; there are 16 beam lines, 4 of which are used in SR lithography. The light from AURORA penetrates two 200-μm beryllium (Be) windows and, within the exposure chamber, uses light with a 0.15- to 0.95-nm wavelength domain. The outline of the beam line is shown in Figure 3. For beam line number 13 (Bl-13), the distance from the light source to the sample is 3.388 m. The exposure environment in the chamber was helium (He) gas at 1 atm to prevent the attenuation of X-rays by N_2 or O_2 gases and to prevent damage to the mask or resist by heat generated during exposure. Figure 4 shows the wavelength and photon density after penetration of the two 200-μm Be windows; the peak wavelength was 0.37 nm.
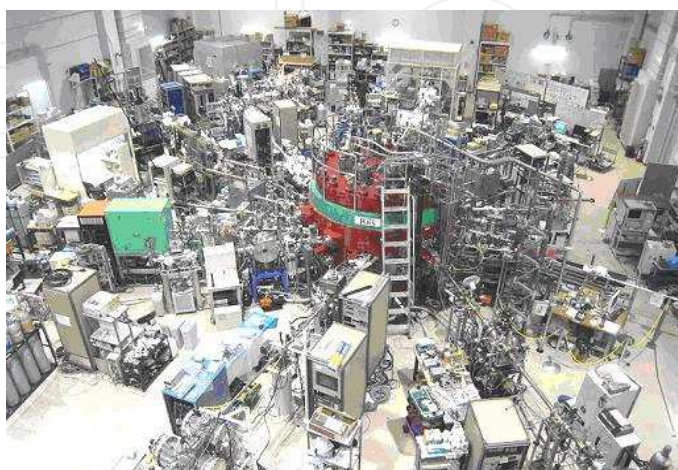

Fig. 2. Superconductivity compact SR source "AURORA" at the SR Centre of Ritsumeikan University in Japan
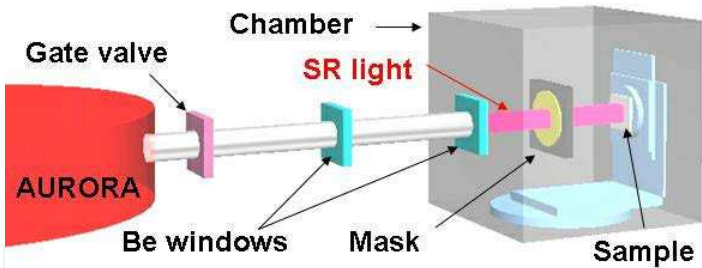
Fig. 3. The outline of the beam line; since wavelengths of 0.2 to 0.5 nm are most suitable for SR lithography, the light from AURORA penetrates two 200-μm Be windows and, within the exposure chamber, uses light with a 0.15- to 0.95-nm wavelength domain
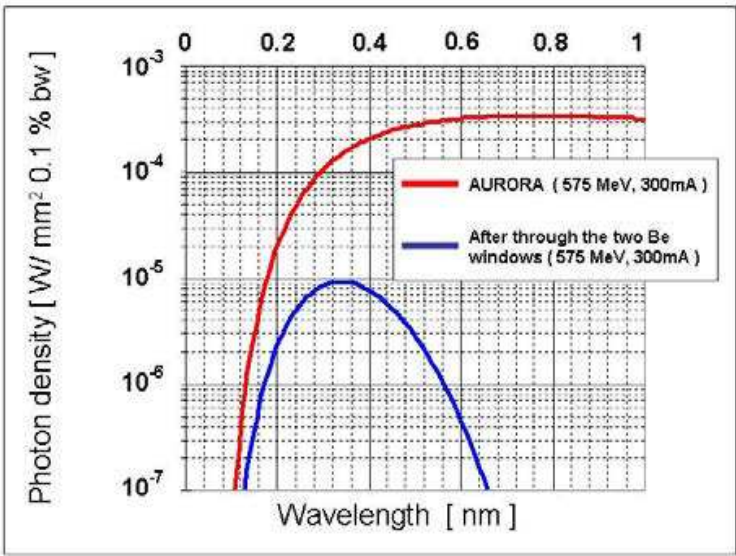

Fig. 4. Relationship between wavelength and photon density after penetration of the two 200-μm Be windows

2.2.2 X-ray mask

Masks used in SR lithography consist of an X-ray absorber, a high-permeability membrane that supports it, and a frame that forms the entire mask. Figure 5A shows the typical structure of an X-ray mask. It is necessary for an X-ray mask to have high contrast to fabricate structures with the required thickness (Singleton & Detemple, 2003; Suzuki & Sugiyama, 1997). As shown in Figure 5B, the mask contrast indicates the ratio of energy through the "membrane only" to energy through the "membrane and absorber."

The primary requirements of X-ray mask membranes include (1) high X-ray transmission, (2) moderate tensile stress, high Young's modulus and high mechanical strength, (3) strong X-ray exposure resistance, and (4) a low rate of thermal expansion. To meet these requirements, Ti, Be, Si_3N_4, SiC, and polyimide are typically used as membrane materials. Although Si_3N_4 and SiC are becoming mainstream, the production cost of X-ray masks based on these materials is high. Thus, polymer materials with low production costs, such as polyimide, are often used as membranes.

The primary requirements for X-ray absorbers of X-ray masks include (1) high X-ray absorptance, (2) a low rate of thermal expansion and no membrane strain, (3) high

processing accuracy, and (4) the ability to fabricate high-aspect-ratio structures. To meet these requirements, heavy metals such as Au, Cu, W, and Ta are typically used as X-ray absorber materials. In general, X-ray absorptance increases with increasing atomic number. Additionally, it is possible to fabricate Au or Cu using electroforming. Because the absorptance of Cu in the X-ray region is lower than that of Au, a Cu absorber must be thicker and have a higher aspect ratio to achieve the same contrast. Therefore, fabrication of Cu is difficult. On the other hand, it is possible to pattern W or Ta using RIE.

Experiments described in this article utilized an X-ray mask consisting of a polyimide membrane with a thickness of 50 μm and an Au absorber with a thickness of 3 μm. The X-ray mask was from Optnics Precision Co., Ltd. The linear expansion coefficient of polyimide is very low compared with other organic compounds and is close to that of metals; therefore, thermal expansion produces low strain when polyimide combines with a metal absorber.
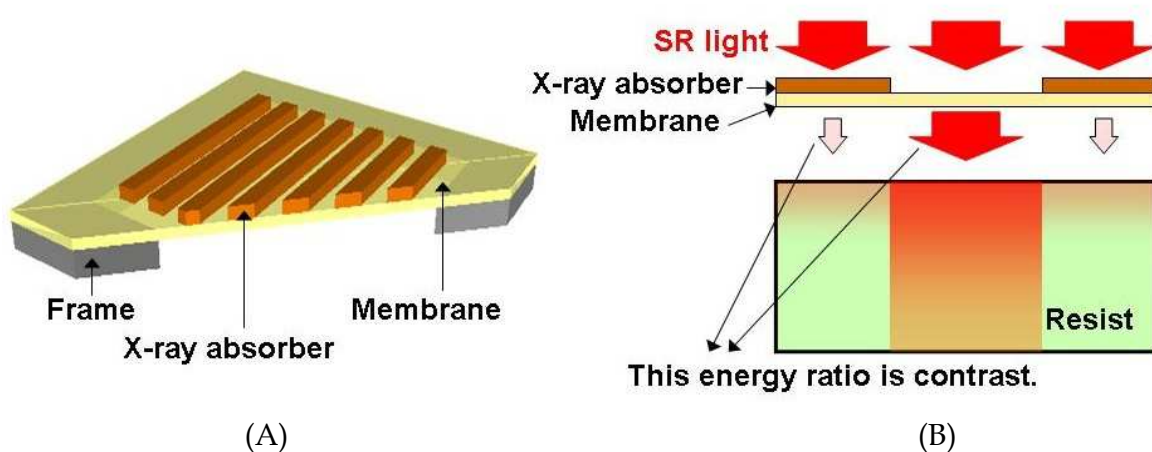

Fig. 5. X-ray mask; (A) typical structure of an X-ray mask; and (B) the mask contrast indicates the ratio of energy through the "membrane only" to energy through the "membrane and absorber"

2.2.3 Resist

When some types of polymer materials are exposed to light, the exposed areas undergo a photochemical reaction, and molecular structures are changed. There are three primary types of photochemical reactions: cross-linking, polarity change, and main-chain breaking. It is possible to design a wide variety of resist materials using these various reaction mechanisms. Additionally, there are two major classes of resist materials: positive resists, in which non-exposed areas are not dissolved after development, and negative resists, in which exposed areas are not dissolved after development.

In general, polymer materials that have high sensitivity and X-ray resolution are suitable as X-ray resists. Most polymer materials used as electron beam resists are not exposed to visible or ultraviolet (UV) light. Therefore, X-ray resists are often used as electron beam resists. Further requirements of X-ray resists include a lack of exposure to small amounts of X-rays through the absorber for fabricating high-aspect-ratio structures and high mechanical strength to endure prolonged exposure and electroforming. To meet these requirements, polymethylmethacrylate (PMMA) is typically used as the X-ray resist.
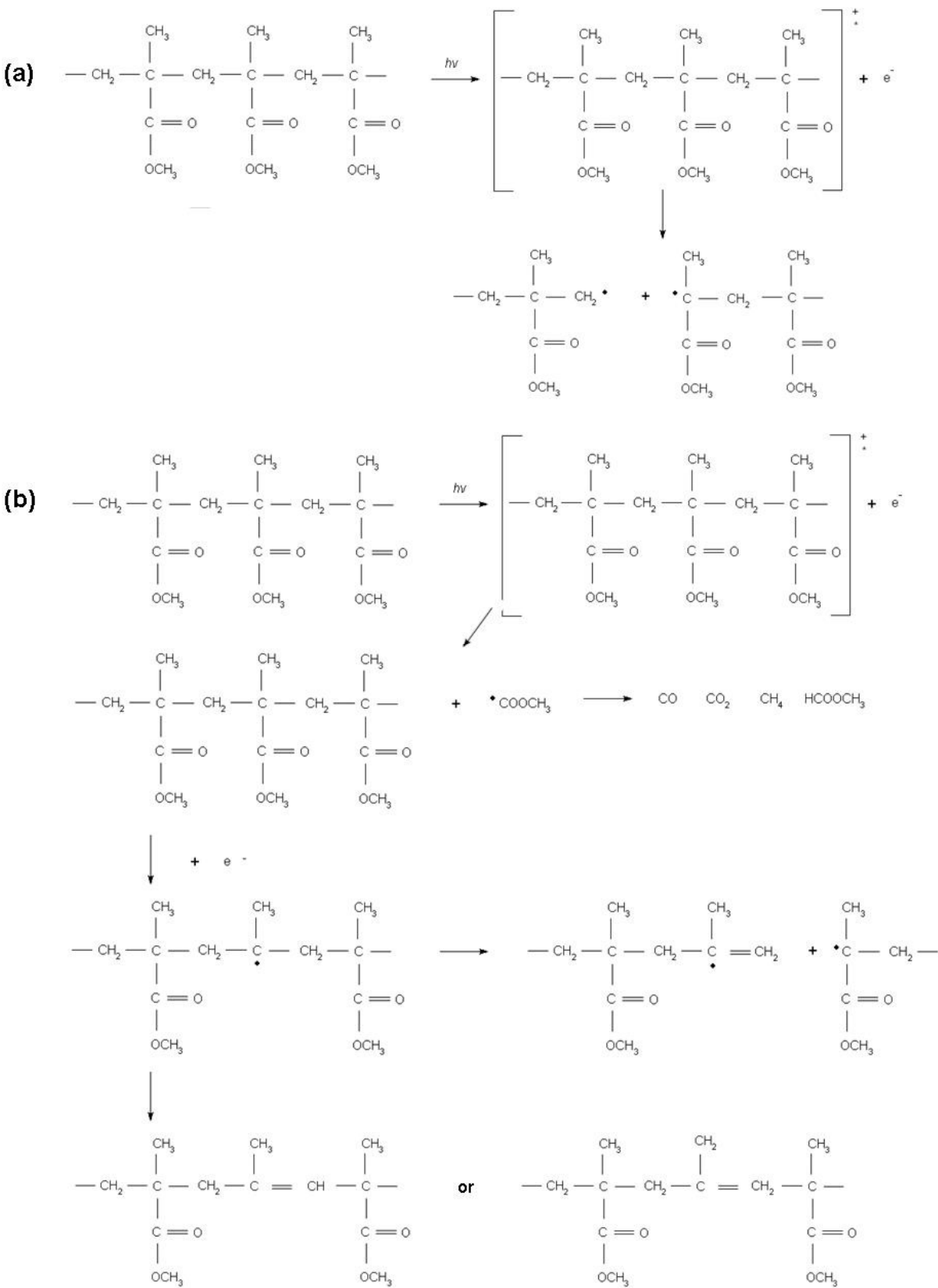
Fig. 6. Photodegradation reaction mechanisms; (A) main-chain breaking without side-chain cleavage; and (B) main-chain breaking via side-chain cleavage

Although the sensitivity of PMMA is low, its resolution is very high (50 Å), and reproducibility of fine structures for moulding can be enhanced by further processing. PMMA is a material in the acrylic plastic group that has a broad range of applications, including lenses, instrument windows, signboards, displays, etc. Among the aforementioned photochemical reactions, PMMA preferentially causes main-chain breaking. If main-chain breaking occurs, molecular mass decreases, and solubility in the developer increases. PMMA has a distinguished transparency and weatherability in many polymer materials. Additionally, because PMMA also has good formability, its mechanical properties are also good. Because PMMA is a malleable optical material, it is possible to use fabricated microstructures directly as optical devices. Experiments described in this article utilized PMMA sheets provided by Nitto Jushi Kogyo Co., Ltd. Figure 6 shows photodegradation reaction mechanisms (Schmal et al., 1996). Figure 6A shows main-chain breaking without side-chain cleavage, and Figure 6B shows main-chain breaking via side-chain cleavage.

2.2.4 X-ray absorbed energy

This section describes absorbed energy in the PMMA resist after exposure. To achieve highly accurate microfabrication or 3-D fabrication, it is necessary to calculate the absorbed energy distribution in the resist. To calculate the absorbed energy in the vertical direction, the following factors must be considered: the photon density spectrum of SR light, attenuation by distance from the light source to the resist, divergence of light, and attenuation when light is transmitted through Be windows. If the spectrum of synchrotron orbital radiation is set to $P_s(\lambda)$, the absorption of the resist is given by the following formula.

$$\Delta P_R(\lambda) = -d/dz\{P_s(\lambda) \cdot T_w(\lambda) \cdot T_M(\lambda) \cdot \exp(-\mu(\lambda)z)\} \tag{1}$$

$T_W(\lambda)$ is the transmissivity in the constituent factor of a beam line until it reaches the front of a mask, such as the Be window and exposure to atmospheric gas, $T_M(\lambda)$ is the transmissivity of the membrane of a mask, $exp(-\mu(\lambda)x)$ is the attenuation in depth x to the inside of the resist, and $\mu(\lambda)$ is an absorbing coefficient of the resist. Moreover, the exposure energy I integrates with the synchrotron orbital radiation spectrum in the wavelength range (0.15–0.95 nm).

$$I = \int_{0.15}^{0.95} P_s(\lambda) \cdot d\lambda \tag{2}$$

The exposure energy after polyimide membrane (50 μm) penetration, I_{Poly}, computed using the conditions described in Section 2.2.2, is given by the following formula.

$$I_{Poly} = \int_{0.15}^{0.95} S_{poly}(\lambda) \cdot d\lambda = 1.587 \times 10^2 \text{ [mJ/sec mA mm}^2] \tag{3}$$

The exposure energy density is given per second and milliamp; thus, if the dosage is applied under the experimental conditions, the arbitrary exposure energy per unit area [mJ/mm²] can be calculated. The penetration energy spectrum $S_{PMMA}(x)$ in arbitrary depth x inside PMMA is given by Formula 4. Additionally, the exposure energy at an arbitrary depth x in PMMA $E_{PMMA}(x)$ is given by Formula 5.

$$S_{PMMA}(x) = S_{Poly}(\lambda) \times \exp(-\mu_{PMMA}(\lambda)x_{PMMA}) \tag{4}$$

$$E_{PMMA}(x) = \int_{0.15}^{0.95} S_{PMMA}(x) \cdot d\lambda \tag{5}$$

The penetration energy spectrum $S_{PMMA}(x)$ was differentiated by the depth direction, and the absorbed energy spectrum $S_{ABS}(x)$ of PMMA was calculated.

$$S_{ABS}(x) = d/dx\, S_{PMMA}(x) = S_{poly}\left\{\exp\left[-\mu_{PMMA}(\lambda)(x_{PMMA} + \Delta x)\right] - \exp\left(-\mu_{PMMA}(\lambda)x_{PMMA}\right)\right\} \tag{6}$$

Therefore, the absorbed energy $E_{ABS}(x)$ at the arbitrary depth x is given by the following formula.

$$E_{ABS}(x) = \int_{0.15}^{0.95} S_{ABS}(x) \cdot d\lambda = \int_{0.15}^{0.95} d/dx S_{PMMA}(x) \cdot d\lambda = E_{PMMA}(x + \Delta x)d\lambda - E_{PMMA}(x) \cdot d\lambda \tag{7}$$

The amount of absorbed energy in PMMA after SR was transmitted through the mask was calculated (Figure 7). The amount of absorbed energy [J/s·mA·mm³] to a depth x [µm] when SR penetrated the membrane (50-µm-thick polyimide) was approximated as $F_{poly}(x)$, and the amount of absorbed energy after SR penetrated the membrane (polyimide) and the absorber (3-µm-thick Au) was approximated as $F_{poly+Au}(x)$.
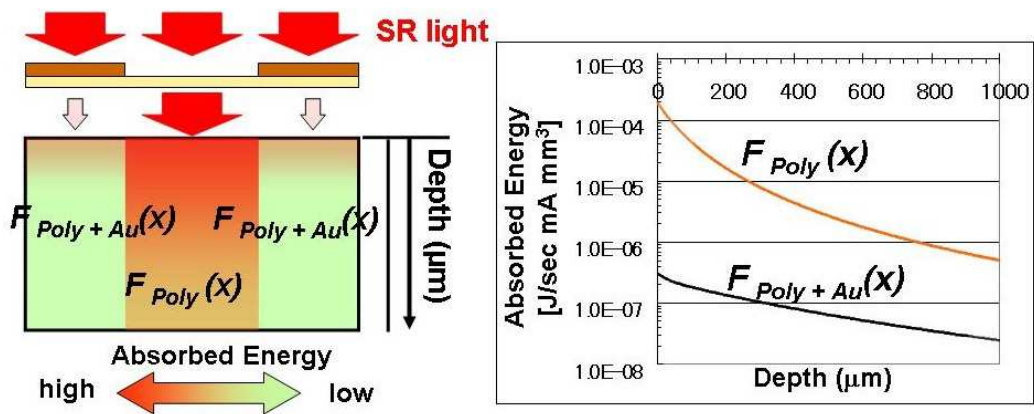

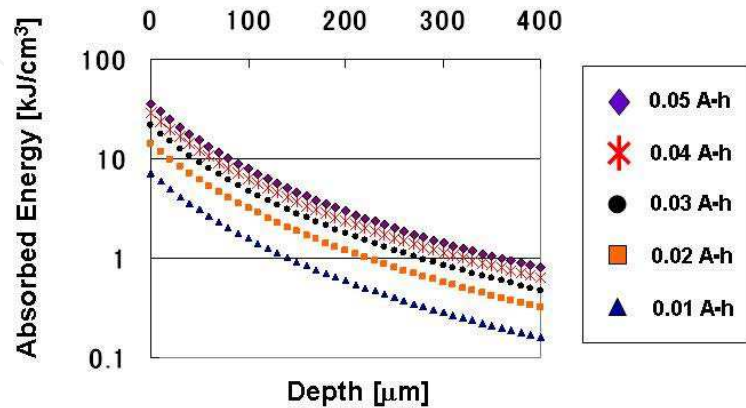Fig. 7. Amount of absorbed energy in PMMA after SR was transmitted through the mask was calculated

Fig. 8. Relationship between depth and absorbed energy

We multiplied $F_{poly}(x)$ and $F_{poly+Au}(x)$ by the dosage, an exposure condition, and the amount of absorbed energy that was actually exposed was calculated. Because the dose was 1 A·h = 3,600,000 mA·s, multiplication of $F_{poly}(x)$ and $F_{poly+Au}(x)$ by the dosage (converted to mA·s) results in a unit of [kJ/cm³]. The relationship between depth and absorbed energy can be calculated from $F_{poly}(x) - F_{poly+Au}(x)$ (Figure 8).

2.3 Development

An important consideration of resist development is the etching rate ratio of the exposed area to the non-exposed area. The developer must select a ratio that decreases the etching rate of the non-exposed area and increases the etching rate of the exposed area. Experiments described in this article utilized GG developer (60 vol% 2-(2-butoxy-ethoxy) ethanol; 20 vol% tetra-hydro-1, 4-oxazine; 5 vol% 2-amino-ethanol-1; and 15 vol% water). Next, stopper liquid (80 vol% 2-(2-butoxy-ethoxy) ethanol and 20 vol% water) was used for 10 min, followed by rinsing with water for another 10 min. All processes were performed at exactly 37°C. PMMA was exposed, and its molecular mass decreased due to a photochemical reaction. Although the molecular mass of PMMA is usually between 10^5 and 10^6 g/mol, it began to dissolve in GG developer when its molecular mass reached 10^4 g/mol.
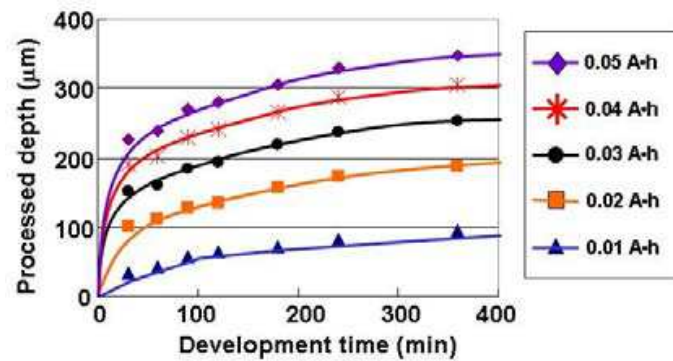

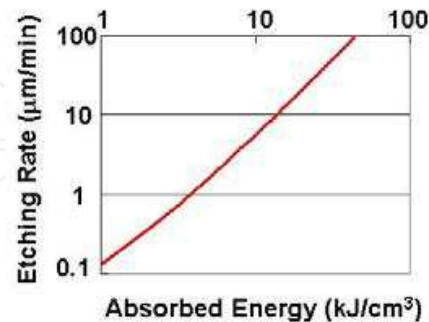Fig. 9. Relationship between development time and processed depth

Fig. 10. Relationship between the absorbed energy and the etching rate

The relationship between development time and processed depth was investigated experimentally (Figure 9). The relationship between the absorbed energy and the etching rate is shown Figure 10. Etching rate is proportional to the amount of absorbed energy. In general, when the development temperature was high, the etching rate, and thus the processing depth, increased. Figure 11 shows the relationship between dosage and

processed depth at a development time of 180 min. Figures 9 and 11 show the experimental values and formula approximations. The processing depth is determined by the dosage and development time, as shown in Figures 9 and 11. Thus, it is possible to determine the processing depth using these approximation formulas.
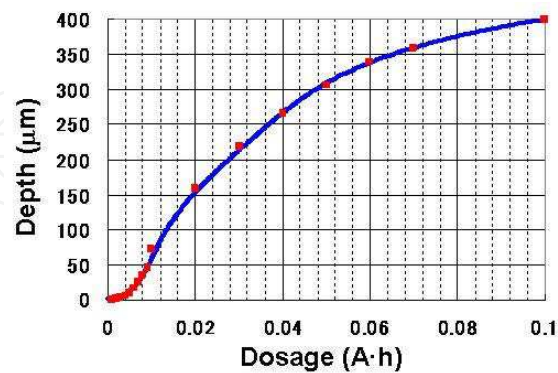

Fig. 11. Relationship between dosage and processed depth at a development time of 180 min

2.4 Approaches to high-accuracy microfabrication
This section describes important parameters that are necessary for high-accuracy microfabrication.

2.4.1 Resolution
The effect of Fresnel diffraction on resolution is determined by wavelength and the gap between the mask and resist surface, whereas the effect of secondary electrons on resolution is determined by wavelength (Figure 12). To transfer a narrow line pattern, it is necessary to narrow the gap between the mask and the resist surface.
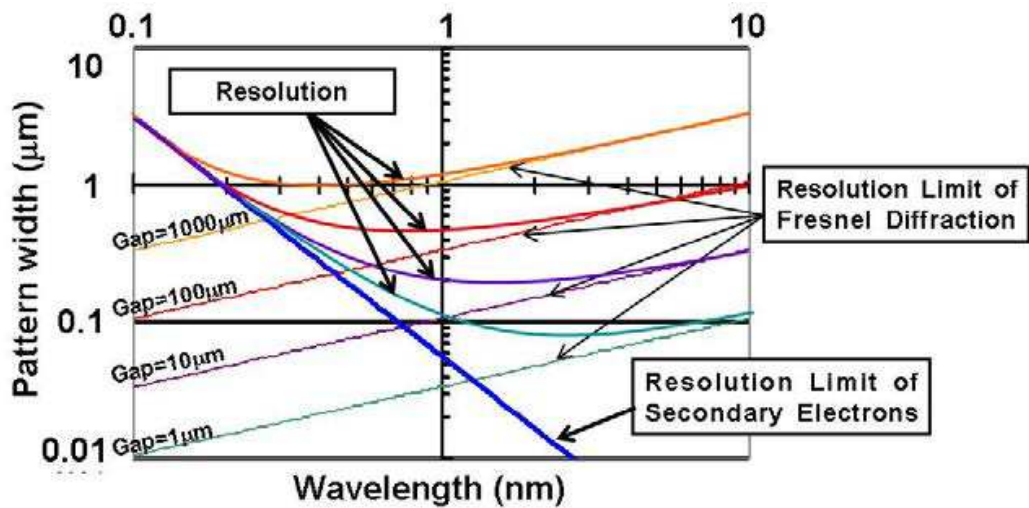

Fig. 12. Relationship between wavelength and pattern width

2.4.2 Optimum experimental conditions
As mentioned in Section 2.3, the processing depth is determined by the dosage and development time and increases with increasing development temperature. For example, to

increase processing depth, even when the dosage is small, the development time or temperature must increase. On the other hand, when the dosage is high, the development time can be short. However, to achieve high-accuracy microfabrication, it is necessary to determine optimum experimental conditions.

When the dosage is too high, bubbles often form inside the resist, especially near the surface. Figure 13 shows a microscopic photograph of damage to the PMMA sheet after exposure. Figure 13B shows exposed microchannel patterns. As seen in the figure, bubbles spread not only to the exposed area but also to the non-exposed area. We confirmed that bubbles influenced the structure after development. Because bubbles often form when the amount of absorbed energy exceeds 80 kJ/cm^3, it is necessary to select a dosage that does not exceed this "surface-damage energy amount."

As mentioned in Section 2.3, the molecular mass of PMMA must be below a certain value in order for PMMA to dissolve in developer. The minimum energy required for dissolution is called the "development-limit energy amount." Although the development limit energy amount varies in the literature, it is approximately 1 kJ/cm^3 based on previous experiments. Variation in the literature values is due to differences in the molecular mass of the PMMA. As the depth from the surface increases, the absorbed energy decreases exponentially; thus, it is necessary to consider not only the surface-damage energy amount but also the development-limit energy amount to determine the optimum dosage.

Next, we discuss the development temperature. As mentioned in Section 2.3, the etching rate increases with increasing development temperature. Because of the higher development temperature and faster etching rate, the processing depth may become large in a short amount of time. However, when the development temperature is too high, the etching rate increases, but the development-limit energy amount decreases. Thus, it is necessary to select the optimum development temperature (Fujinawa et al., 2006). If the development-limit energy amount is too low, PMMA resist develops not only in the exposed area, but also in the non-exposed areas (through the absorber). Therefore, sloped-sidewall structures are fabricated. On the other hand, when the development temperature is low, the processing depth is low, and a long development time is required. Because PMMA swells in water, a long development time is a disadvantage. For these reasons, the development process was performed at 37°C.
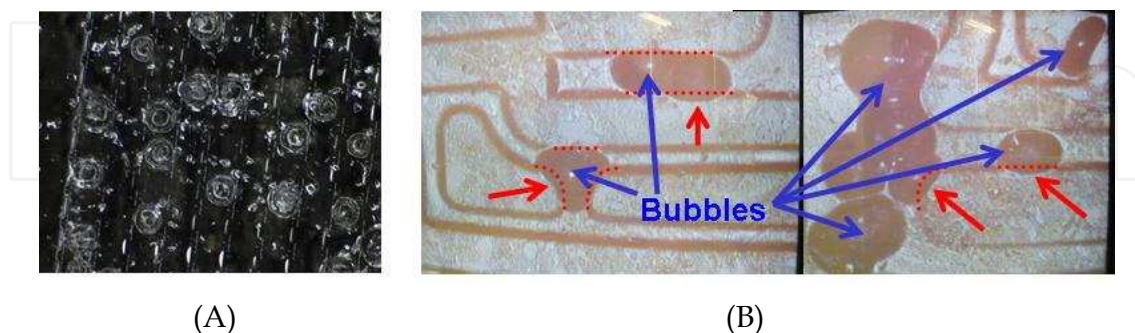

(A)   (B)

Fig. 13. Microscope photographs of damaged to the PMMA sheet after exposure

2.4.3 Micro-loading effect

In this section, the influence of the micro-loading effect is described. The micro-loading effect is a phenomenon that leads to different processing depths depending on the line width. If the line width is narrow, circulation of the developer worsens, it is difficult to

supply new developer to the bottom, and dissolved PMMA tends to remain near the bottom. Figure 14 shows the relationship between line width and processing depth using dosages of 0.03 and 0.05 A·h. Plots show experimental values for line widths of 10, 15, 20, and 25 μm, and lines show the processing depth of the domain where the line is wide. Figure 15 shows the percentage of processing depths that reached the domain where the line is wide. As shown in Figures 14 and 15, processing depth decreased with decreasing line width. However, higher percentages of processing depth where the line is wide correspond to longer development time. That is, although developer circulation was reduced, dissolution progressed slowly. When the dosage was low, the percentage was high. Additionally, the processing depth was low, and thus the circulation of the developer was good. However, as shown in Figure 14B and C, when the line width was too narrow, dissolution did not progress slowly. Thus, when narrow line patterns are transferred, it is necessary to consider the influence of the micro-loading effect.
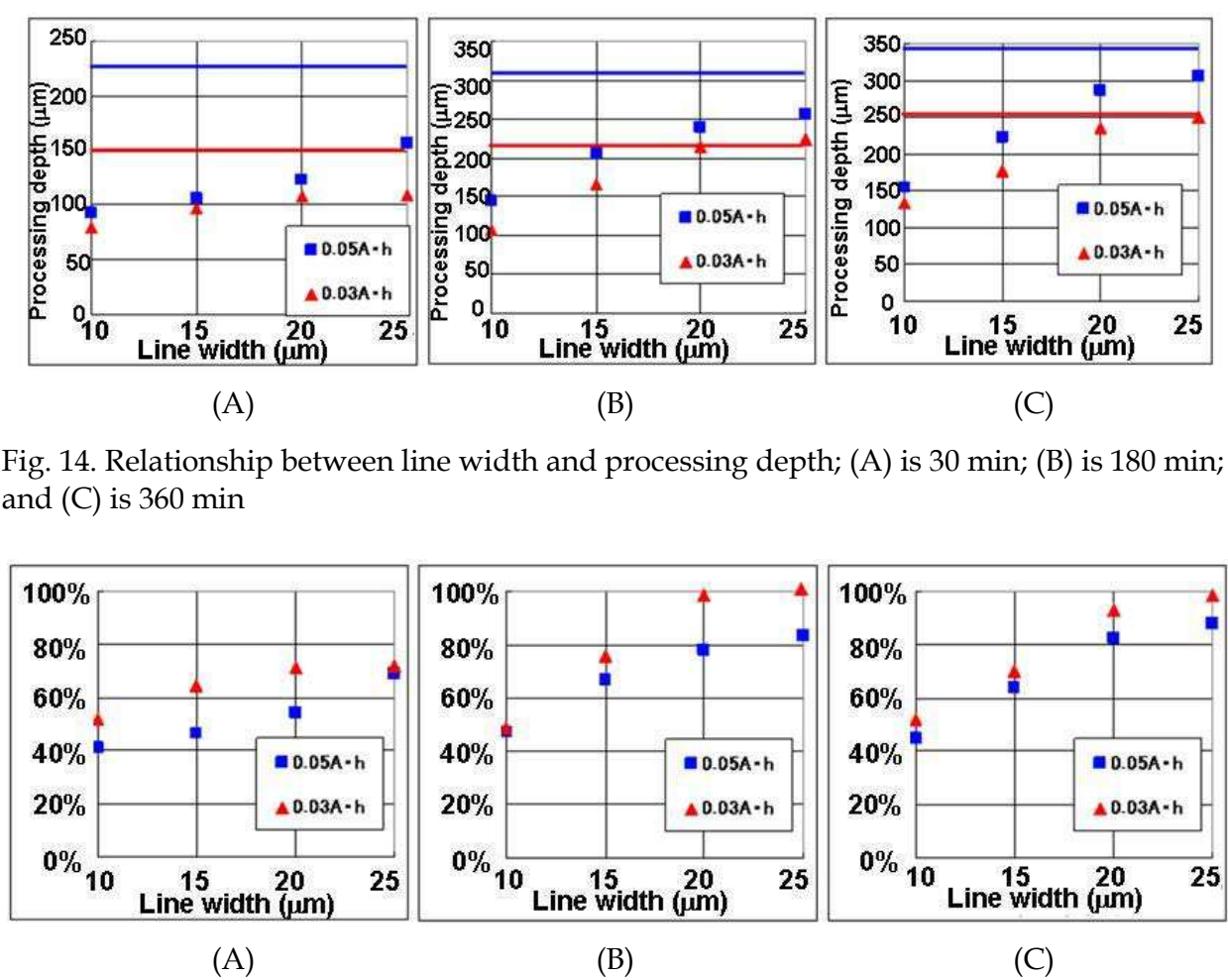

Fig. 14. Relationship between line width and processing depth; (A) is 30 min; (B) is 180 min; and (C) is 360 min

Fig. 15. Percentage of processing depths that reached the domain where the line is wide; (A) is 30 min; (B) is 180 min; and (C) is 360 min

3. 3-D fabrication method

This section describes the fabrication of 3-D structures using SR lithography. In this article, two fabrication methods are described in detail: the plain-pattern to cross-section transfer

(PCT) technique and the pixels exposure technique. When the PCT technique is used, it is possible to fabricate a microneedle array structure (Khumpuang et al., 2006). When the pixels exposure technique is used, it is possible to fabricate a 3-D structure with a complex surface, such as an asymmetrical structure.

3.1 Advancement in the LIGA process

As mentioned in Section 2.3, a characteristic of SR lithography is that it is possible to fabricate a thick structure, and the processing depth can be controlled by dosage. Thus, it was expected that SR characteristics could be applied to the fabrication technology of 3-D structures with free-form surfaces or sloped sidewalls. Additionally, studies on 3-D processing methods using the LIGA process have been reported previously. "SLIGA" adds a sacrificial layer process to the LIGA process. Although the traditional LIGA process can only fabricate a mechanical component fixed to the substrate, the SLIGA technique enables fabrication involving sensors with moving parts (Ruzzu et al., 1998). For example, fabrication of a high-aspect-ratio microactuator was reported. However, this processing technique produces structures with sidewalls that are vertical to the resist surface. To control the inclination angle of the sidewall, the "skew exposure technique" is used to incline resists for X-rays during exposure (Tsuei et al., 1998; Ehrfeld et al., 1999). However, the structures that can be fabricated are limited, and fabrication of structures with free-form surfaces is not possible. Recently, methods that give energy distributions to the resist surface, such as grayscale mask UV lithography, have been reported. If complicated energy distributions can be given to resist surfaces, it will be possible to fabricate complicated arbitrary 3-D structures.
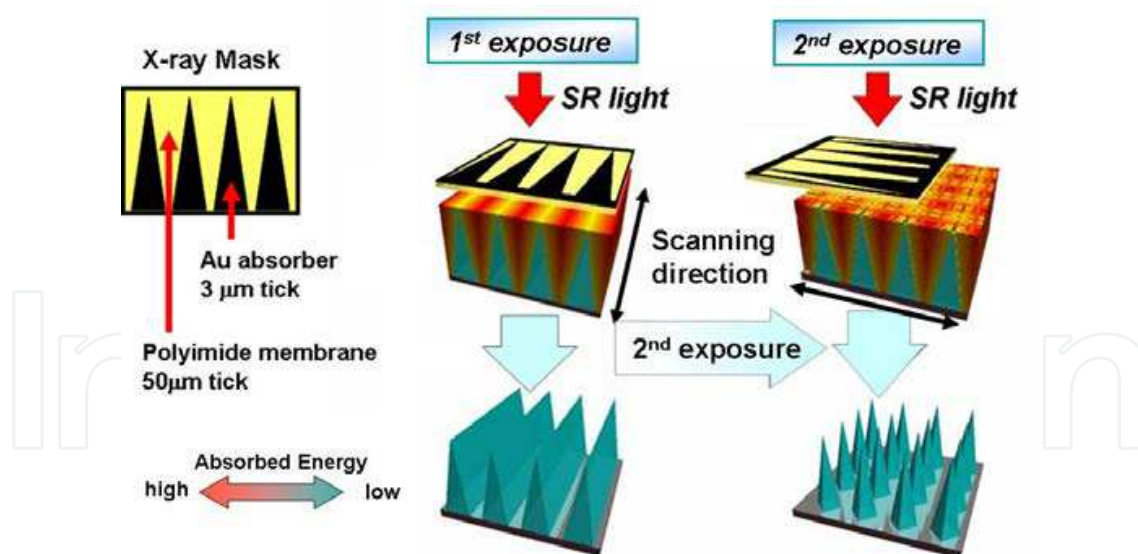

Fig. 16. PCT technique, black color shows X-ray absorber and corn color shows membrane, energy amount is shown by shading, the energy distribution is deposited in the resist by scanning, and a more complex energy distribution can be given by rotating the mask 90°

3.2 PCT technique

Figure 16 shows the PCT technique. The energy distribution is deposited in the resist by scanning, as shown in the figure. Three-dimensional structures were fabricated by

subsequent development. Additionally, a more complex energy distribution can be given by rotating the mask 90°. For example, a needle shape can be fabricated using the PCT method. When the PCT technique is used, a shape similar to that of the mask absorber pattern is expected to be fabricated. Therefore, if the exposure distribution onto the resist is expected to form a curved shape or sloped-sidewall structure whose cross-section is similar to the mask absorber pattern as the target shape. As shown in Figure 16, when the PCT technique is used, it is possible to fabricate a microneedle array structure, as indicated by the diagram below. If this method is used, it is possible to fabricate both a microneedle and microlens array. Fabrication results of 3-D structures are shown in Figure 17.

(A)   (B)   (C)
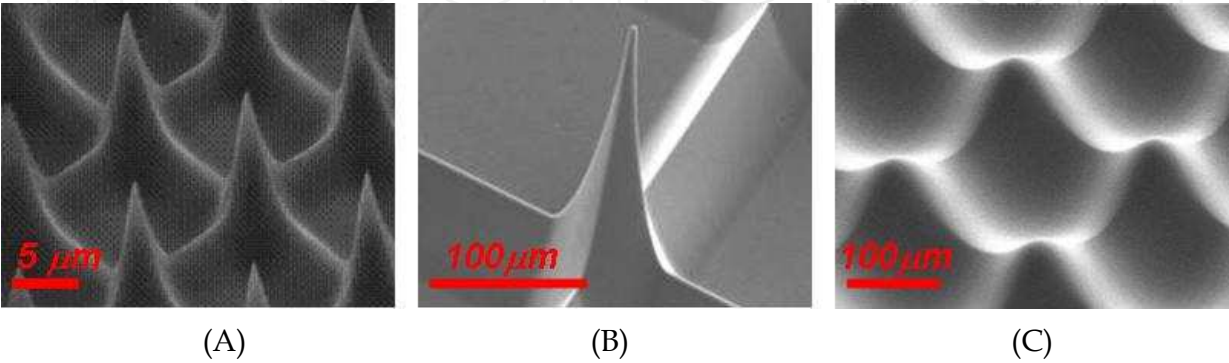
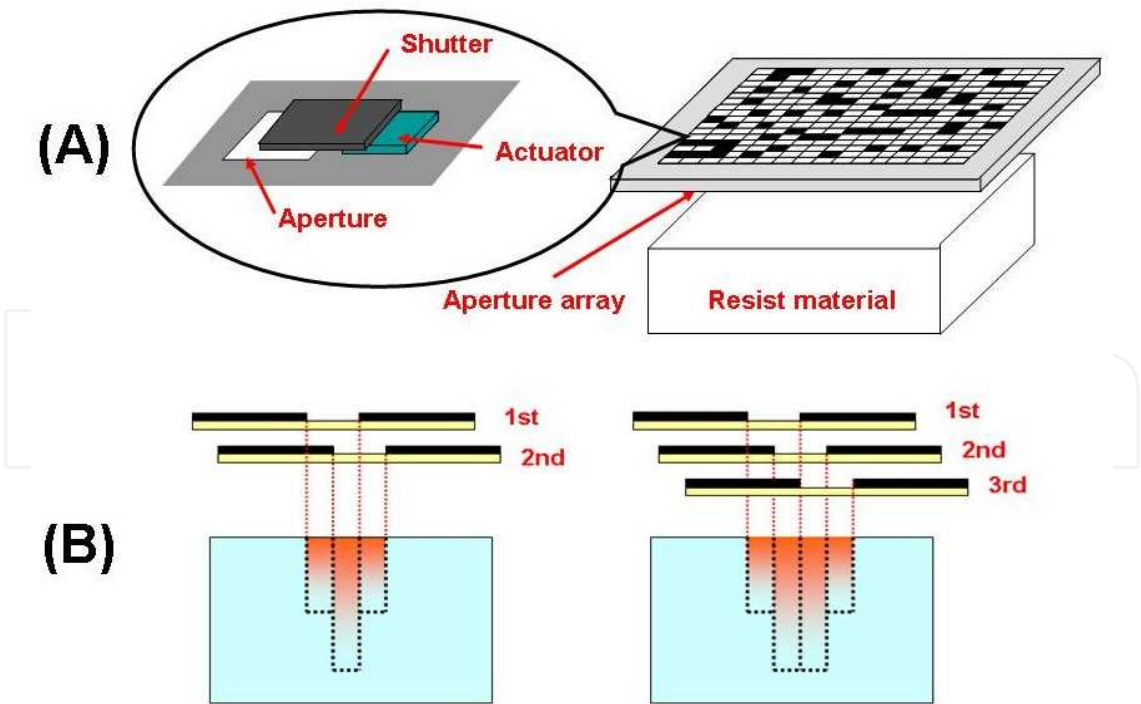Fig. 17. Fabrication results of 3-D structures

Fig. 18. Pixels exposure technique; (A) SR light is shaped by the aperture, and the amount of exposure energy is controlled by opening and closing the aperture with an actuator; and (B) an ideal mosaicked exposure energy by two-axis scanning of the PMMA resist
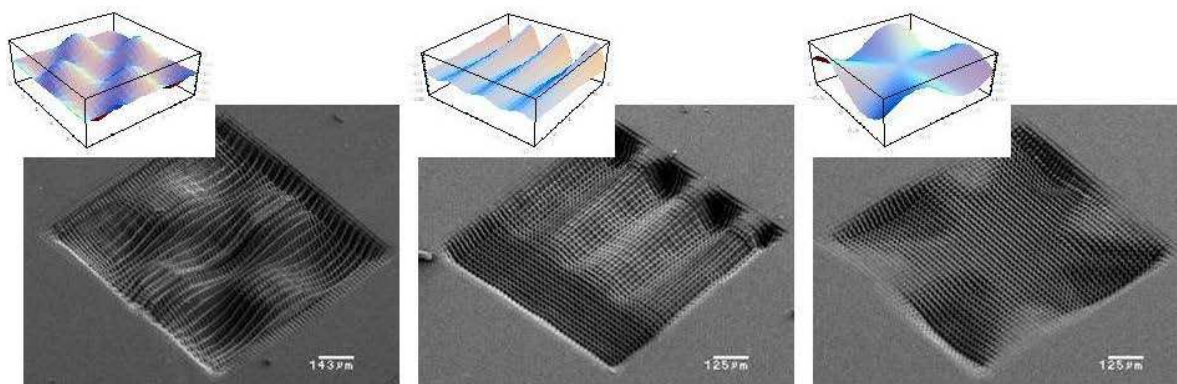
Fig. 19. The target forms and fabrication structures

3.3 Pixels exposure technique

With the pixels exposure technique, it is possible to fabricate arbitrary 3-D microstructures using a mask with an appropriate pattern. In this technique, SR light is shaped by the aperture, and the amount of exposure energy is controlled by opening and closing the aperture with an actuator (Figure 18A). This technique applies the energy distribution in a mosaicked shape, as shown in the figure. Because the array was difficult to fabricate, we fabricated a 20-μm-thick, 75- × 80-μm single aperture made of Ni to distribute an ideal mosaicked exposure energy by two-axis scanning of the PMMA resist (Figure 18B). Because fabrication masks were not needed and it is suitable for rapid prototyping, fabrication time and cost were reduced. When the PMMA resist is exposed to a mosaicked energy distribution with the same aperture size, a smooth free-form surface cannot be fabricated. Thus, because the resolution of PMMA is very high, if even a few adjoining pixels overlap or there is a gap between pixels, channels or pillars appear on the boundary surface. Based on these basic studies, fabrication of structures with smooth free-form surfaces was achieved using an exposure method in which the pixels were overlapped beforehand. Moreover, an algorithm to determine the amount of exposure energy while taking overlap into consideration was written for the target form to fabricate a 3-D structure that had an arbitrary shape. The target forms and fabrication structures are shown in Figure 19.

4. PTFE fabrication by SR ablation

This section describes 3-D PTFE microstructures fabricated by SR ablation. Advantages of ablation technology and the mechanism of fabrication are described.

4.1 PTFE

PTFE is a fluoroplastic material known for its excellent material characteristics, including insulation against high voltages, resistance to chemicals and creep, and high thermal stability. PTFE was discovered in 1938 by Dr. Roy J. Plunkett, who was a researcher of E.I. du Pont de Nemours and Company, a commercial reality in 1946. PTFE is best known by the DuPont brand name Teflon®. In addition to its primary use in non-stick frying pans and filters, PTFE is also used in a broad range of fields, such as those involving household articles, OA equipment, semiconductors, and cars. Despite its long (> 60-year) history, new uses for PTFE are developed continuously because of its outstanding characteristics. Because PTFE has excellent material characteristics, it is expected to be applicable to MEMS.

4.2 Microfabrication of PTFE

PTFE microfabrication is difficult to achieve. It is impossible to fabricate this material through wet etching with chemicals (acids and alkali) used in numerous microfabrication techniques, such as lithography, because of its excellent chemical resistance. Additionally, when the temperature is increased above the melting point of PTFE (327°C), the viscosity becomes too high for moulding. Moreover, laser ablation, which has been widely used in recent years as an effective tool for direct microfabrication, is also difficult. Because the first absorption band of PTFE is near 160 nm, where little light is absorbed by the UV to infrared (IR) domain, ablation processing using a laser with this domain is not possible. Most laser processing of PTFE is not laser ablation but rather thermal processing, which causes a deformation in structure surfaces. Therefore, lasers with narrower wavelengths, such as vacuum ultraviolet (VUV) pulsed-lasers or ultrashort pulsed-lasers, are used for microfabrication of PTFE. However, the aspect ratio of the structures that can be fabricated is very small, generally <1. For these reasons, laser ablation was developed, replacing lasers with SR light.

4.3 SR ablation

In 1996, a technique for direct etching of PTFE using an SR light source was reported (Katoh & Zhang, 1996). Unlike X-ray lithography, direct etching was performed entirely with dry etching and did not use wet etching. With this technology, it is also possible to combine the electroforming technique and moulding process, as in the LIGA process. This technology is referred to as the TIEGA™ (Teflon® Included Etching Galvanic Forming) process. Figure 20 shows the process flow of the TIEGA™ process. The etching rate of PTFE using SR ablation is very high, 10–100 μm/min. Moreover, because the developing process is not necessary, structure collapse is not caused by sticking effects. Sticking is problematic in microfabrication utilizing wet etching, such as lithography. Although fabrication of high-aspect-ratio structures is also possible, surface roughness of sidewalls is undesirable, and the taper angle is large compared with that of the LIGA process.
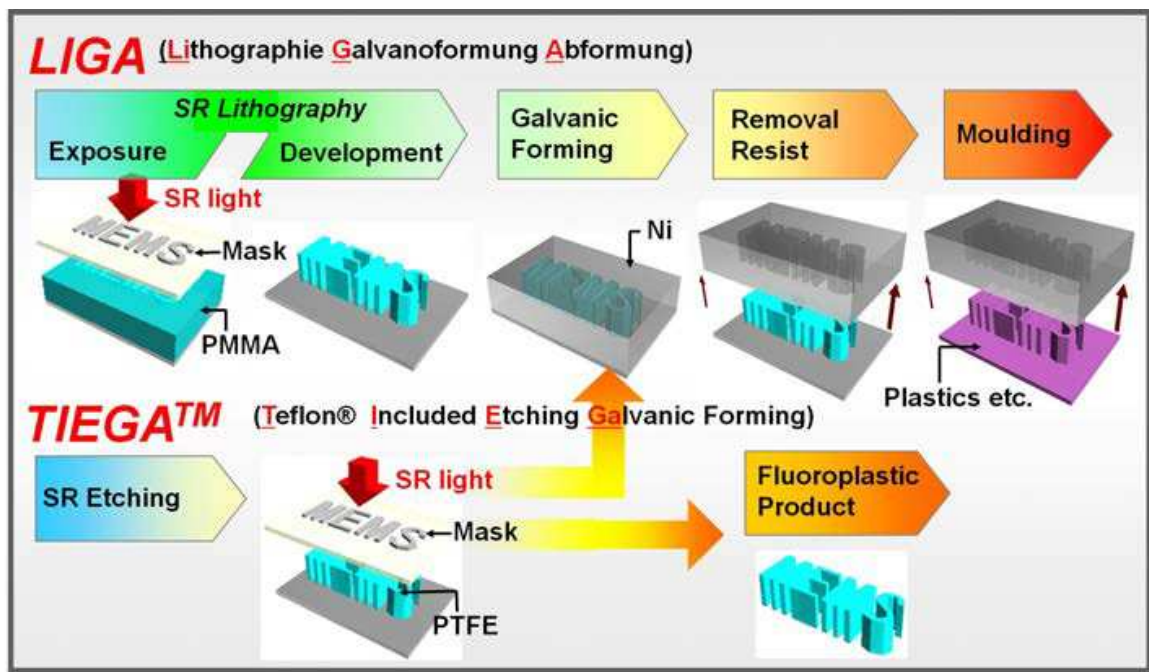

Fig. 20. Process flow of the TIEGA™ process

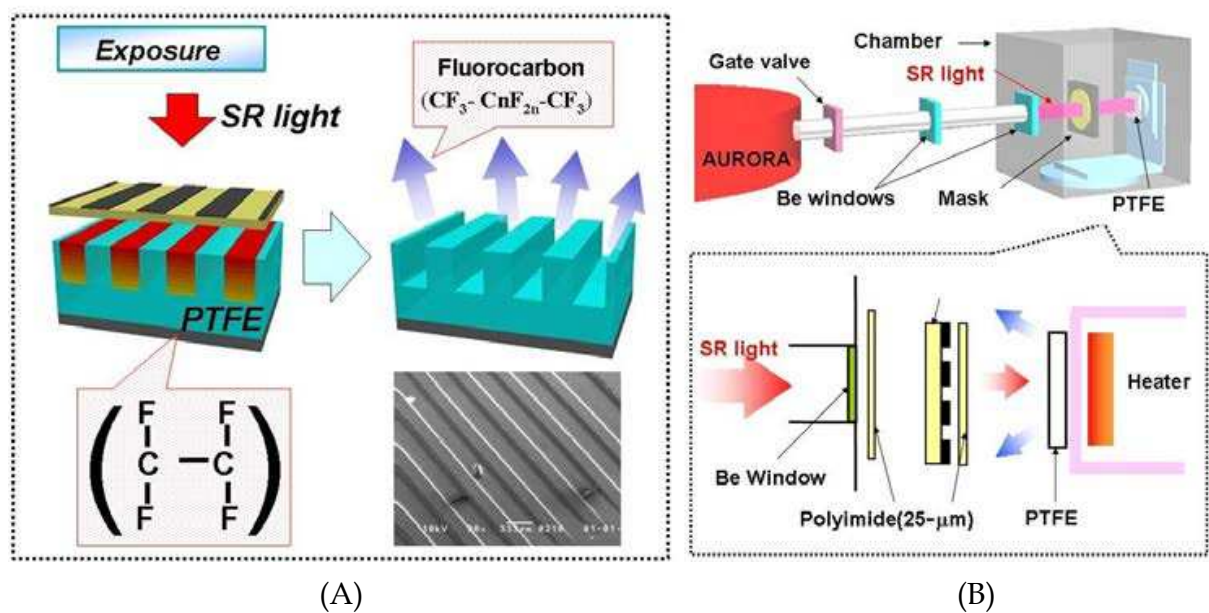(A)   (B)

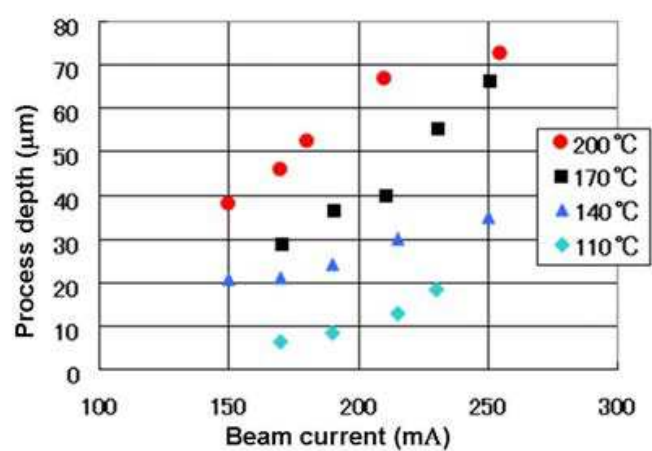Fig. 21. (A) is processing mechanism; and (B) is experimental system

Fig. 22. Relation between the beam current and processing depth

We used a 1-mm-thick product from Yodogawa Hu-tech Co., Ltd. for PTFE. The processing mechanism is outlined in Figure 21A. When PTFE is exposed to an SR light source, a photochemical reaction occurs in which the main chain of the material decomposes, forming a fluorocarbon gas (CF_3-C_nF_{2n}-CF_3), and exposed parts are etched. The etching rate generally increases when PTFE is etched in a vacuum chamber and heated during the SR ablation fabrication process. The secession rate of fluorocarbon gas increases if the PTFE temperature is excessively high at this time. Therefore, a vacuum atmosphere at 10^{-5} torr was used, and a substrate heater was installed in the chamber. To prevent the mask and Be window from becoming contaminated by fluorocarbon gas, a 25-μm polyimide film was placed on each (Figure 21B). The processing depth was checked after an exposure of 30 min, and the PTFE surface temperature was increased to 110°C, 140°C, 170°C, and 200°C in succession. Figure 22 shows the relationship between the beam current and processing depth. In general, the TIEGA™ process utilizes white light. However, because this experimental system was

designed for use with the TIEGA™ process as well as the LIGA process, PTFE was only exposed to the X-ray domain. Therefore, the etching rate and processing depth were low.

4.4 3-D Fabrication of PTFE

Because the PCT technique successfully provided PMMA 3-D structures, we adapted the PCT technique to expose PTFE while the stage was in motion. Fabrication of 3-D PTFE microstructures using other techniques has also been reported, including 3-D PMMA structures (Nakamura and Tabata, 2006; Nishi et al., 1999). Figure 23 shows 3-D PTFE structures fabricated using the PCT technique with a triangular mask pattern. Figure 23A shows a structure in which the PTFE surface temperature was 140°C, and Figure 23B shows a structure in which the PTFE surface temperature was 200°C. As shown in the figure, higher PTFE temperatures correspond to enhanced surface roughness. Figure 24 shows the target forms and 3-D PTFE structures fabricated using the PCT technique with other mask patterns.

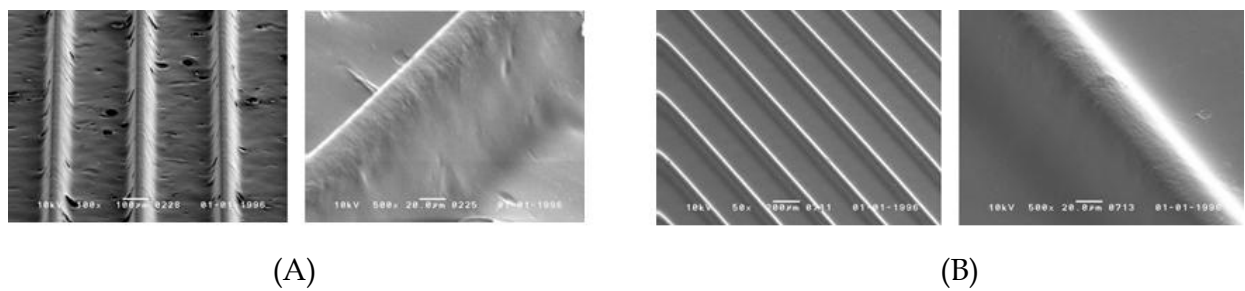(A)   (B)

Fig. 23. 3-D PTFE structures fabricated using the PCT technique with a triangular mask pattern; (A) PTFE surface temperature was 140°C; and (B) PTFE surface temperature was 200°C
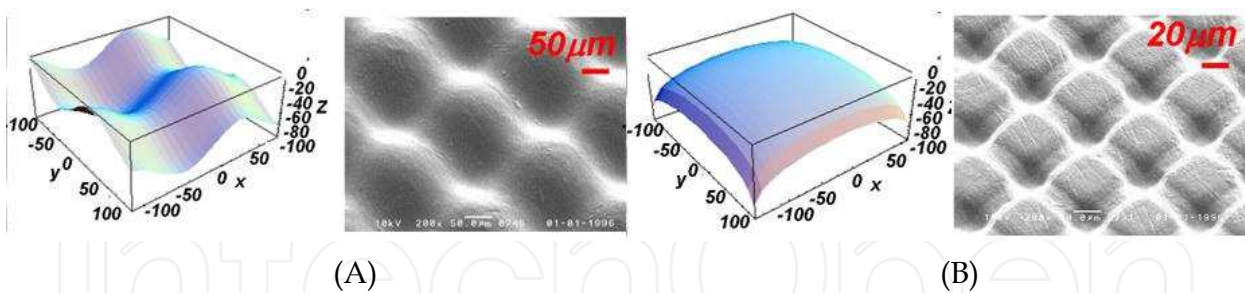

(A)   (B)

Fig. 24. Target forms and 3-D PTFE structures fabricated using the PCT technique with other mask patterns; (A) is utilizing sine-curved mask pattern; and (B) is utilizing semicircular mask pattern

5. Conclusions

MEMS devices have attracted much attention, and further studies are needed to realize their full potential. In fabrication technology, an elemental technology, microfabrication, developed primarily using a semiconductor process, is in high demand. Recently, MEMS devices have diversified, and microfabrication technologies for the production of high-aspect-ratio and 3-D structures are in demand. This article described the fabrication of 3-D microstructures utilizing SR lithography.

Chapter 1 (Introduction) described the field of fabrication technologies of high-aspect-ratio structures and 3-D structures and explained the purpose of SR lithography. Chapter 2 (SR Lithography) provided an outline of the LIGA process, fabrication mechanism of SR lithography, processing-depth control, and optimum experimental conditions. Sections 2.2 (Exposure) and 2.3 (Development) described the mechanism of SR lithography and the requirements of the light source, the X-ray mask, and the resist materials. Section 2.4 (Approaches to High-Accuracy Microfabrication) described the resolution, optimum experimental conditions, and micro-loading effect based on both experimental and theoretical values. To achieve high-accuracy microfabrication, all of these are important. Chapter 3 (3-D Fabrication Method) described the fabrication method of 3-D structures utilizing SR lithography. Two fabrication techniques were described in detail: the PCT technique and the pixels exposure technique. In this chapter, the fabrication process and results, as well as the mechanism of 3-D fabrication, were described. Chapter 4 (PTFE Fabrication by SR Ablation) described the 3-D PTFE microstructures fabricated by SR ablation. Advantages of ablation technology and the fabrication mechanism were described. We expect that this research will contribute to elemental technologies in the field of MEMS, the achievement of high functionality, and to the development of high-performance devices that, so far, have been difficult to realize.

6. Acknowledgment

7. References

Ehrfeld, W.; Wood, R.L.; Hessel, V.; Lowe, H.; Schulz, C ; Weber, L (1998), Materials of LIGA technology, *Microsystem Technologies*, Springer, Vol.5, Num.3, pp.105-112, ISSN 0946-7076

Fujinawa, S.; Kato, F.; Sugiyama, S (2006), Development of fabrication process for shape-control of three-dimensional submicron structure by synchrotron radiation lithography, *Proceedings of SPIE - The International Society for Optical Engineering*, Vol.6037, pp.331-338,, ISSN 0277-786X, Brisbane, Australia, Dec.11-15,2005

Horade, M. & Sugiyama, S (2010), Study on fabrication of 3-D microstructures by synchrotron radiation based on pixels exposed lithography, *Microsystem Technologies*, Springer, Vol.16, Num.8-9, pp.1331-1338, ISSN 0946-7076

Kato, F.; Fujinawa, S.; Li, Y.G.; Sugiyama, S (2007), Fabrication of a spiral microcoil using a 3D-LIGA process, *Microsystem Technologies*, Springer, Vol.13, Num.3-4, pp.221-225, ISSN 0946-7076

Kato, T. & Zhang, Y (1998), High aspect ratio micromachining by synchrotron radiation direct photo-etching, *Microsystem Technologies*, Springer, Vol.4, Num.3, pp.135-138, ISSN 0946-7076

Kondo, R.; Takimoto, S.; Suzuki,K.; Sugiyama, S (2000), High aspect ratio electrostatic micro actuators using LIGA process, *Microsystem Technologies*, Springer, Vol.6, Num.6, pp.218-221, ISSN 0946-7076

Kumpuang, S.; Horade, M.; Fujioka, K.; Sugiyama, S (2006), Microneedle fabrication using the plane pattern to cross-section transfer method, *Smart materials and structures,* Vol.15, Institute of Physics, pp.600-606, ISSN 0964-1726

Lee, K.C & Lee, S.S (2003), 3D fabrication using deep X-ray mask with integrated micro-actuator, *Proceedings of 16th IEEE International conference on Micro Electro Mechanical Systems (MEMS 2003)*, pp.558-561, ISBN 0-7803-7744-3, Kyoto, Japan, Jan 19-23, 2003

Matsuzuka, N.; Hirai, Y.; Tabata, O (2004), A novel fabrication process of 3-D microstructures by double exposure in standard deep X-ray lithography, *Proceedings of 17th IEEE International conference on Micro Electro Mechanical Systems (MEMS 2004)*, pp.681-684, ISBN 0-7803-8265-X, Maastricht, Netherlands, Jan 25-29, 2004

Mekaru, H.; Kusumi, S.; Sato, N.; Shimizu, M.; Yamashita, M.; Shimada,O.; Hattori, T (2007), Fabrication of a spiral microcoil using a 3D-LIGA process, *Microsystem Technologies*, Springer, Vol.13, Num.3-4, pp.393-402, ISSN 0946-7076

Nakamura, Y. & Tabata, O (2006), Moving Mask Direct Photo-Etching (M2DPE) for 3D Micromachining of Polytetrafluoroethylene, *IEEJ Transactions on Sensors and Micromachines,* Vol.126, Num.9, pp.499-503, ISSN 1347-5525

Nishi, N.; Katoh, T.; Ueno, H.; Kohish, S.; Sugiyama, S (1999), 3-Dimensional Micromachining of PTFE Using Synchrotron Radiation Direct Photo-Etching, *Proceedings of the 1999 International Symposium on Micromechatronics and Human Science*, Vol.5148, pp.93-98, ISBN 0-7803-5790-6, Nagoya, Japan, Nov 23-26, 1999

Ruzzu, A.; Fahrenberg, J.; Heckele, M.; Schaller, T (1998), Fabrication of a spiral microcoil using a 3D-LIGA process, *Microsystem Technologies*, Springer, Vol.4, Num.3, pp.128-131, ISSN 0946-7076

Schmalz, O.; Hess, M.; Kosfeld, R (1996), Structural changes in poly(methyl methacrylate) during deep-etch X-ray synchroton radiation litography, *Die Angewandte makromolekulare Chemie*, Num.239, pp.63-78, ISSN 0003-3146

Singleton, L& Detemple, P (2003), Mask technologies for deep x-ray LIGA, *Proceedings of SPIE - The International Society for Optical Engineering*, Vol.5148, pp.210-217, ISSN 0277-786X

Sugiyama, S.; Khumpuang, S.; Kawaguchi, G. (2004), Plain-pattern to Cross-section Transfer (PCT) Technique for Deep X-ray Lithography and Applications, *Journal of Micromechanics and Microengineering*, Vol.14, pp. 1399-1404, ISSN : 0960-1317

Suzuki, K. & Sugiyama, S (1997), Silicon IC compatible LIGA mask-fabrication process, *Microsystem Technologies*, Springer, Springer, Vol.4, Num.1, pp.7-11, ISSN 0946-7076

Tabata, O.; Matsuzuka, N.; Yamaji, T.; Uemura, S.; Yamamoto, K (2002), 3D fabrication by moving mask deep X-ray lithography (M2DXL) with multiple stages, *Proceedings of 15th IEEE International conference on Micro Electro Mechanical Systems (MEMS 2002)*, pp.180-183, ISBN 0-7803-7185-2, Las Vegas, USA, Jan 20-24, 2002

Tsukada, N.; Nakao, T. & Higuchi, T. (2005), 3D microstructures fabrication of paraffin or plastics with laser heating, *Proceedings of 18th IEEE International conference on Micro Electro Mechanical Systems (MEMS 2005)*, pp.576-579, ISBN 0-7803-8732-5, Miami, USA,Jan 30- Feb 3, 2005

Ueno, H.; Zhang, Y.; Nishi, N.; Sugiyama, S (2000), Fabrication of sub-micron structures for MEMS using deep X-ray lithography, *Microsystem Technologies*, Springer, Vol.6, Num.6, pp.210-213, ISSN 0946-7076
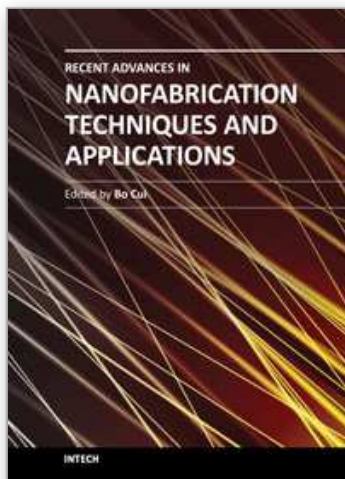
Recent Advances in Nanofabrication Techniques and Applications

Edited by Prof. Bo Cui

Nanotechnology has experienced a rapid growth in the past decade, largely owing to the rapid advances in nanofabrication techniques employed to fabricate nano-devices. Nanofabrication can be divided into two categories: "bottom up" approach using chemical synthesis or self assembly, and "top down" approach using nanolithography, thin film deposition and etching techniques. Both topics are covered, though with a focus on the second category. This book contains twenty nine chapters and aims to provide the fundamentals and recent advances of nanofabrication techniques, as well as its device applications. Most chapters focus on in-depth studies of a particular research field, and are thus targeted for researchers, though some chapters focus on the basics of lithographic techniques accessible for upper year undergraduate students. Divided into five parts, this book covers electron beam, focused ion beam, nanoimprint, deep and extreme UV, X-ray, scanning probe, interference, two-photon, and nanosphere lithography.

How to reference

In order to correctly reference this scholarly work, feel free to copy and paste the following:

INTECH
open science | open minds